Effect of Hydrogen on the Fracture Mechanisms of Tempered Martensitic Steels

L. Cupertino-Malheiros[a,b], D. Guedes[b], A. Oudriss[a], F. Decultieux[b], F. Thébault[b], J. Bouhattate[a], J. Creus[a], X. Feaugas[a]

a. Laboratoire des Sciences de l'Ingénieur pour l'Environnement, UMR CNRS 7356, Université de La Rochelle, Avenue Michel Crépeau, 17042 La Rochelle Cedex 0, France
b. Vallourec Research Center France, 60 route de Leval, F-59620 Aulnoye-Aymeries, France

Abstract
Using an assembly of a permeation test on a tensile machine, this work aims to study the effect of hydrogen combined with several mechanical states on the fracture of two martensitic steels. The designed mechanical tests followed by FEM modelling is an efficient method to investigate the impact of hydrostatic stress and plasticity to the fracture process. A correlation was found between quasi-cleavage zones and the highest levels of plastic strain and hydrostatic stress. Additionally, mobile hydrogen enhanced the plasticity contribution to the fracture process significantly.

Key words: fracture mechanism; hydrogen embrittlement; lath martensite; FEM modelling

Introduction
In the recent years, there is a demand for high-strength steels with enough hydrogen embrittlement (HE) resistance for offshore oil and gas exploitation [1, 2]. The study of hydrogen-induced fracture is necessary in order to develop tempered martensitic steels that comply with the new strength and HE resistance requirements of the oil industry.
In lath martensitic steels, hydrogen embrittlement depends on the hydrogen fugacity, the susceptibility of the steel and the service mechanical request [3]. Notched specimens introduce stress triaxiality, affecting the ductility and the damaging mechanisms of alloys [4]. Hydrogen can be located at the lattices or trapped at different structural features [5]. Its concentration, distribution and diffusion are strongly affected by the steel structure and the hydrostatic stress distribution.
This work studies the susceptibility to hydrogen embrittlement of two martensitic steels tested with different mechanical states (several notches geometries) and hydrogen concentrations. A permeation cell on a tensile machine and an elastoplastic model together with FEM calculations are used in this investigation.

Experimental Procedure
This work studies cylindrical and prismatic notched specimens of two tempered martensitic steels with 0.3%C and additions of Si, Mn, Cr, Mo, V and Nb provided by Vallourec Research Center France. The main compositional difference is the Mo content. According to this difference, they are named HM (higher molybdenum) and LM (lower molybdenum) steels.
For the cylindrical specimens, the hydrogen pre-charging was performed by polarizing cathodically the specimens for 24 hours in a 1mol/L H_2SO_4 solution as shown in Figure 1(a).

For the prismatic specimens, both pre-charged and under hydrogen flux tests were performed in a permeation cell assembled directly on the tensile machine as illustrated in Figure 1(b). Solutions of 1mol/L H_2SO_4 and 0.1mol/L NaOH were respectively employed in the charging and detection cells.
In both tests, charging current densities from -20 to -100mA/cm^2, saturated sulfate reference electrode SSE (Hg/Hg2SO4/K2SO4) and platinum counter electrode were used. The temperature was fixed to 20°C and the cells were kept under argon flux.
Mechanical testing was performed in an INSTRON 100kN machine with a strain rate of $10^{-5}s^{-1}$ until fracture.

Figure 1 : Photo and scheme of (a) electrochemical charging of cylindrical specimens and (b) permeation assembly on the tensile machine.

FEM Calculations and Elastoplastic Model

The model uses a function $f(\bar{\bar{\sigma}})$ as a plasticity yield criterion where $f(\bar{\bar{\sigma}}) = 0$ is a state at the border of the domain. Equation 1 shows how this function is calculated based on the von Mises equivalent stress (σ_{eqVM}), the yield strength σ_Y and three hardening terms R_0, X_1 and X_2 (where R_0 is isotropic and X_1 and X_2 are kinematic components).

$$f(\overline{\overline{\sigma}}) = \sigma_{eqVM} - [\sigma_Y + R + X_1 + X_2] \quad (1)$$

Elastic Regime - When $f(\bar{\bar{\sigma}}) < 0$, the state $(\bar{\bar{\sigma}})$ is inside the elastic domain and can be calculated by Equation 2. In this equation, C is a fourth order tensor that describes the isotropic elasticity. The deformation is obtained as a function of the transformation gradient tensor $\overline{\overline{Fe}}$ by using Equation 3.

$$\bar{\bar{\sigma}} = C : \bar{\bar{\varepsilon}}_e \quad (2)$$

$$\bar{\bar{\varepsilon}} = \frac{1}{2}(\overline{\overline{Fe^T}}\,\overline{\overline{Fe}} - \bar{\bar{I}}) \quad (3)$$

Plastic Regime - When $f(\bar{\bar{\sigma}}) = 0$ the state $(\bar{\bar{\sigma}})$ is inside the plastic domain. In this case, the von Mises equivalent stress can be obtained by Equation 1 once the yield strength and the hardening terms (R_0, X_1 and X_2) are known.

The hardening terms can be calculated by Equation 4, where S and Z are empirical constants that are obtained by fitting experimental tensile curves.

$$A_i = \frac{S_i}{Z_i}\left[1 - \exp\left(-Z_i\, \varepsilon_{peq}\right)\right] \tag{4}$$

In this equation, $A_i \in \{R_0, X_1, X_2\}$ and $i \in \{0,1,2\}$. Finally, the plastic deformation is calculated using Equation 5 where *K* and *n* are viscosity constants.

$$\overline{\overline{\dot{\varepsilon_p}}} = \left[\frac{f(\overline{\overline{\sigma}})}{K}\right]^n \frac{\partial f(\overline{\overline{\sigma}})}{\partial \overline{\overline{\sigma}}} \tag{5}$$

Results

Figure 2 shows examples of tensile curves illustrating the effect of notch geometry 2(a) and hydrogen 2(b) on the tensile behavior. As expected, the higher the K_t, the higher the stress and the smaller the strain in the tensile curves. The embrittlement effect of hydrogen was also observed with the decrease of the total strain in the tensile curves. Mobile hydrogen presented a greater embrittlement effect than the deeply trapped hydrogen. This embrittlement under hydrogen flux was also seen in the fracture surfaces as quasi-cleavage regions that appear where there are higher levels of hydrostatic stress.

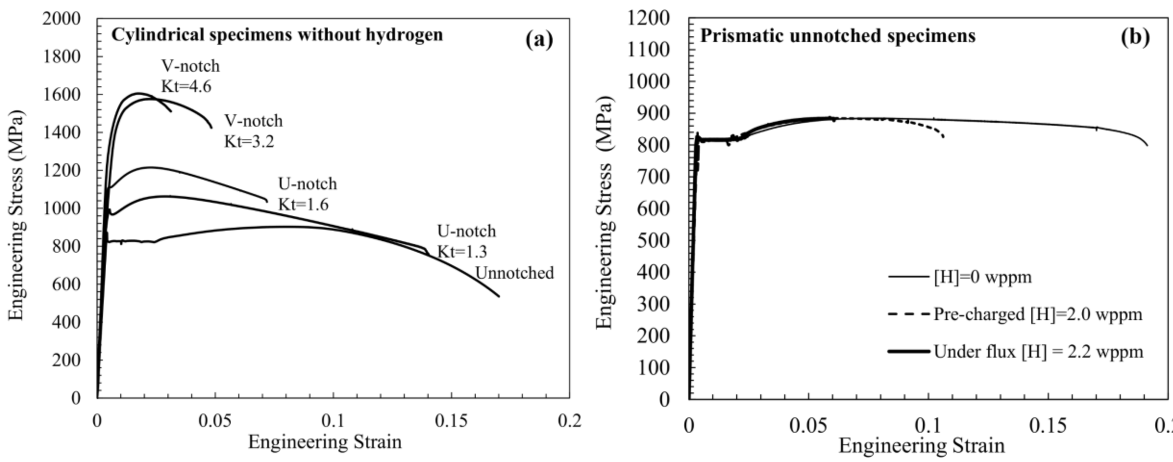

Figure 2: Effect of (a) notch and (b) hydrogen on the tensile curves of the LM steel.

Figure 3 shows the variation of the maximal hydrostatic stress (σ_m) with the equivalent plastic strain (ε_{peq}) for the three tests conditions (air, pre-charged and under hydrogen flux). In the three conditions, the σ_m decreases as a function of the ε_{peq}. Equation 6 represents the macroscopic criterion of fracture used in the present work [6, 7]. In this equation, σ_c is the critical stress for fracture and A is the strain sensitivity parameter.

Table 1 provides the values of σ_c and A obtained by fitting the data to straight lines and using the Equation 6. The increase of the A parameter with hydrogen indicates that hydrogen enhanced the contribution of plasticity to the fracture process, especially the mobile one.

$$\sigma_c = \sigma_m + A\epsilon_{peq} \tag{6}$$

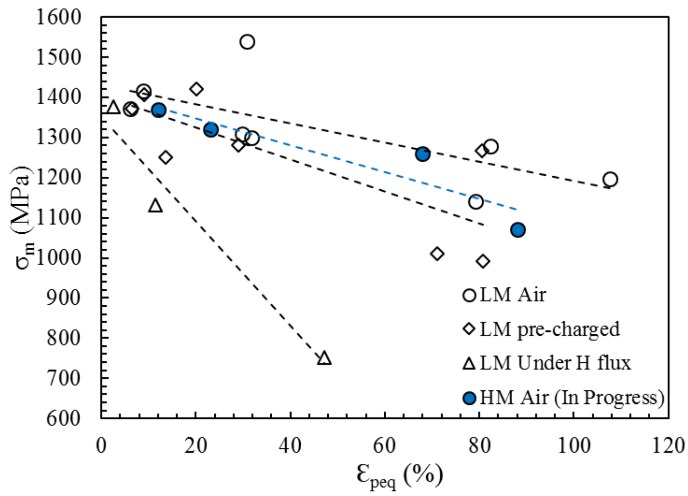

Figure 3 : Evolution of the maximal hydrostatic stress as a function of the equivalent plastic strain for testing on air, after hydrogen pre-charging and under hydrogen flux.

Table 1 : Critical stress for fracture (σ_c) and absolute value of the strain sensitivity parameter (A) for specimens tested on air, after pre-charging and under hydrogen flux.

	LM steel			HM steel (In progress)
Parameters	Air	Pre-charged	Under H flux	Air
σ_c (MPa)	1431	1403	1352	1414
A (MPa)	2.4	4.0	13.0	3.3

Conclusions

The designed mechanical tests (several notch shapes and hydrogen concentrations) followed by the local approach of fracture using FEM modelling provided an efficient method to investigate the impact of the plasticity and hydrostatic stress to the fracture process. Work is currently underway to implement the same methodology to other high-strength steels. The objective is to plot the graph of Figure 3 to other steels in order to classify them according to their susceptibility to trapped and mobile hydrogen.

References

[1] Y. Arai, T. Mochizuki, T. Omura, K. Kondo, S. Yoshida, Study of high-strength low-alloy steel OCTG with high carbon contents for mildly sour service, NACE Corrosion/2017, New Orleans, LA, 26-30 March 2017, paper 9051.

[2] X. Wen, P. Bai, B. Luo, S. Zheng, C. Chen, Review of recent progress in the study of corrosion products of steels in a hydrogen sulphide environment, Corros Sci 139 (2018) 124-140.

[3] J. Venezuela, Q. Liu, M. Zhang, Q. Zhou, A. Atrens, The influence of hydrogen on the mechanical and fracture properties of some martensitic advanced high strengths steels studied using the linearly increasing stress test, Corros Sci 99 (2015) 98-117.

[4] A. L. Helbert, X. Feaugas, M. Clavel, The influence of stress triaxiality on the damage mechanisms in a equiaxed α/β Ti-6Al-4V alloy, Metall Mater Trans A (1996) 3043-3058.

[5] S. Frappart, X. Feaugas, J. Creus, F. Thebault, L. Delattre, H. Marchebois, Study of the hydrogen diffusion and segregation into Fe-C-Mo martensitic HSLA steel using electrochemical permeation test, J Phys Chem Solids 71 (2010) 1467-1479.

[6] F.M. Beremin, “Cavity formation from inclusions in ductile fracture of a508 steel”, Metallurgical Transactions A 12, (1981): p. 723–731.

[7] B.Z. Margolin, V.A. Shvetsova, A.G. Gulenko, V.I. Kostylev, “Prometey Local Approach to Brittle Fracture: Development and Application”, Engineering Fracture Mechanisms 75, (2008): p. 3483-3498.